

# SGHA-Attack: Semantic-Guided Hierarchical Alignment for Transferable Targeted Attacks on Vision-Language Models

Haobo Wang, Weiqi Luo, *Senior Member, IEEE*, Xiaojun Jia, Xiaochun Cao, *Senior Member, IEEE*

**Abstract**—Large vision–language models (VLMs) are vulnerable to transfer-based adversarial perturbations, enabling attackers to optimize on surrogate models and manipulate black-box VLM outputs. Prior targeted transfer attacks often overfit surrogate-specific embedding space by relying on a single reference and emphasizing final-layer alignment, which underutilizes intermediate semantics and degrades transfer across heterogeneous VLMs. To address this, we propose SGHA-Attack, a Semantic-Guided Hierarchical Alignment framework that adopts multiple target references and enforces intermediate-layer consistency. Concretely, we generate a visually grounded reference pool by sampling a frozen text-to-image model conditioned on the target prompt, and then carefully select the Top-K most semantically relevant anchors under the surrogate to form a weighted mixture for stable optimization guidance. Building on these anchors, SGHA-Attack injects target semantics throughout the feature hierarchy by aligning intermediate visual representations at both global and spatial granularities across multiple depths, and by synchronizing intermediate visual and textual features in a shared latent subspace to provide early cross-modal supervision before the final projection. Extensive experiments on open-source and commercial black-box VLMs show that SGHA-Attack achieves stronger targeted transferability than prior methods and remains robust under preprocessing and purification defenses.

**Index Terms**—Adversarial attack, Cross-modal synchronization, Hierarchical alignment, Vision-language models.

## I. INTRODUCTION

Large Vision-Language Models [1] have emerged as a foundational technology, powering critical applications from autonomous agents to content moderation [2]–[4]. As these systems are increasingly entrusted with high-stakes decision-making [5], [6], their inherent vulnerability to adversarial perturbations poses severe security risks [7]. Beyond causing benign classification errors [8], imperceptible perturbations can effectively hijack a model’s semantic understanding, enabling adversaries to circumvent safety guardrails (i.e., jailbreaking) and elicit policy-violating outputs [9]. In the black-box scenario, targeted transfer-based attacks [10] represent a particularly practical threat. By optimizing on an accessible surrogate, attackers can precisely steer proprietary

Haobo Wang and Weiqi Luo are with Guangdong Province Key Lab of Information Security Technology, and School of Computer Science and Engineering, Sun Yat-sen University, Guangdong 510006, China (e-mail: wanghb69@mail2.sysu.edu.cn; luoweiqi@mail.sysu.edu.cn.) Corresponding author: Weiqi Luo.

Xiaojun Jia is with Nanyang Technological University, Singapore (e-mail: jiaxiaojunqaa@gmail.com).

Xiaochun Cao is with the School of Cyber Science and Technology, Shenzhen Campus, Sun Yat-sen University, Shenzhen 518107, China. (e-mail: caoxiaochun@mail.sysu.edu.cn)

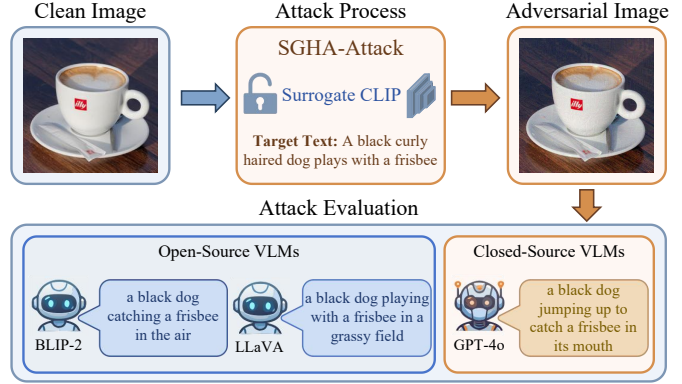


Fig. 1: Illustration of the proposed SGHA-Attack framework targeting diverse VLMs.

commercial APIs to generate specific target captions without knowledge of the victim’s internal parameters. This transferability threatens the integrity of downstream ecosystems, including automated decision support [11] and tool-augmented agentic systems [12]. To unveil the severity of this threat, we introduce SGHA-Attack, as illustrated in Fig. 1, a novel framework designed to effectively mislead diverse black-box VLMs to generate attacker-specified target captions.

Existing transfer-based attacks can be broadly categorized into perturbation-constrained methods and unrestricted diffusion-based approaches. In the constrained category, methods like AttackVLM [13] optimize adversarial perturbations by aligning global image embeddings with a target text embedding within a restricted  $\ell_\infty$  budget. Chain-of-Attack (COA) [14] further enhances this by incorporating modality fusion and iterative optimization strategies to improve semantic consistency. M-Attack [15] introduces robust input transformations, such as random resizing and cropping, to bypass the preprocessing pipelines of commercial models. In the unrestricted category, approaches like AdvDiffVLM [16] leverage latent diffusion models to generate adversarial examples. Specifically, they utilize attention-guided masking to preserve critical features, fundamentally operating by reconstructing image content rather than adding imperceptible noise. Despite different designs, these transfer-based attacks have two common limitations. First, they rely on a single target reference, which can be sensitive to the surrogate model and thus transfer poorly to other VLMs. Second, they match embedding similarity only at the surrogate encoder’s final

layer, ignoring intermediate features, this can cause overfitting to the surrogate and weaken targeted transfer to instruction-tuned or proprietary VLMs.

To address these limitations, we propose SGHA-Attack, a *Semantic-Guided Hierarchical Alignment* framework that enforces target consistency across intermediate-layer representations rather than only at the final output. To tackle the single-target limitation, we introduce Semantic-Guided Anchor Injection (SGAI). Instead of optimizing toward one target reference, SGAI uses multiple semantic anchors that capture diverse realizations of the target concept and forms a weighted mixture of these anchors as the optimization target, making the guidance more stable and improving targeted transfer across different VLMs. To address the second limitation of relying on final-layer matching, we further perform hierarchical alignment over intermediate representations: Hierarchical Visual Structure Alignment (HVSA) constrains layer-wise visual features at multiple intermediate depths, aligning both global and spatial structure, while Cross-Modal Latent Space Synchronization (CLSS) provides intermediate cross-modal supervision in a shared latent subspace by encouraging projected visual features to remain aligned with the evolving textual semantics rather than only at the final output. Together, these designs provide multi-layer supervision and yield adversarial examples with stronger targeted transferability across a wide range of open-source and commercial black-box VLMs.

Our main contributions are summarized as follows:

- We propose SGHA-Attack, a Semantic-Guided Hierarchical Alignment framework for transfer-based targeted attacks on VLMs that moves beyond late-stage embedding matching by enforcing hierarchical, multi-granularity semantic consistency.
- We introduce SGAI to build multiple target references through generation and careful selection (generate an anchor pool and select Top- $K$ ), and leverage HVSA/CLSS to align intermediate visual features and synchronize intermediate cross-modal tokens.
- Extensive experiments on open-source and commercial black-box VLMs show that SGHA-Attack improves targeted transferability over prior methods and remains robust under preprocessing and purification defenses.

## II. RELATED WORK

### A. Vision-Language Models

VLMs have evolved from task-specific architectures to more general-purpose, generative foundation models [1], [17], [18]. Prior to the widespread adoption of large language models (LLMs), many VLMs emphasized learning joint visual–textual representations for discriminative objectives, including image–text retrieval [19], [20] and visual question answering [21], [22]. More recently, the emergence of strong LLMs has shifted the dominant paradigm toward leveraging an LLM as a language and reasoning backbone while introducing a visual front-end that enables the model to condition on images [23], [24]. Under this paradigm, a central technical challenge is modality alignment: mapping visual representations into a

form that an LLM can effectively consume and integrate with text [25], [26].

In practice, modality alignment is commonly implemented via a learnable projector (or adapter) that connects the visual encoder to the LLM. Two representative design families are widely adopted. The first family, exemplified by LLaVA [3] and MiniGPT-4 [27], uses lightweight mappings such as linear layers or MLPs to project visual tokens into the LLM embedding space, offering simplicity and computational efficiency. The second family, used by BLIP-2 [28] and InstructBLIP [29], introduces a query-based module (e.g., Q-Former) that employs learnable queries and cross-attention to selectively aggregate visual information before interfacing with the LLM. In this work, we study adversarial transferability across these architectures, with particular attention to how their alignment modules and intermediate representations influence vulnerability and generalization of attacks.

### B. Adversarial Attacks on VLMs

Adversarial attacks aim to mislead models via imperceptible input perturbations. Depending on the adversary’s knowledge, they are classified as white-box (full parameter access) [30], [31] or black-box (no access to model parameters or gradients) [32], [33]. Regarding objectives, attacks distinguish between untargeted ones that merely degrade performance and targeted ones that steer outputs toward specific malicious goals, posing greater safety risks. In realistic black-box scenarios, transfer-based attacks [34]–[36] have emerged as the dominant paradigm over query-based methods [37], as the latter are often impractical for large VLMs due to prohibitive inference latency and API costs. Consequently, our work focuses on transfer-based targeted attacks, which optimize perturbations on an accessible surrogate (e.g., CLIP) to compromise unseen victim VLMs via cross-model transferability.

Early research on VLM robustness primarily focused on untargeted degradation [38]–[42]. Recently, significant progress has been made in targeted transfer-based attacks. Representative works like AttackVLM [13] craft targeted examples by aligning global image embeddings with a specific target reference. Subsequent methods such as Chain-of-Attack (COA) [14] improve semantic consistency through iterative optimization and modality fusion, while IPGA [43] exploits intermediate projector representations (e.g., Q-Former) for fine-grained alignment. Others, including AdvDiffVLM [16] and M-Attack [15], further enhance transferability via diffusion-based generation or robust input transformations. However, these methods predominantly operate on the encoder’s output or the subsequent projection stage, treating the visual backbone itself as a monolithic feature extractor. This strategy overlooks the rich hierarchical representations within the visual encoder, where features evolve from low-level structures to high-level semantics. In contrast, our work explicitly opens the visual backbone and synchronizes its intermediate hierarchical features with corresponding textual representations, thereby enforcing deep semantic consistency throughout the entire feature extraction process.

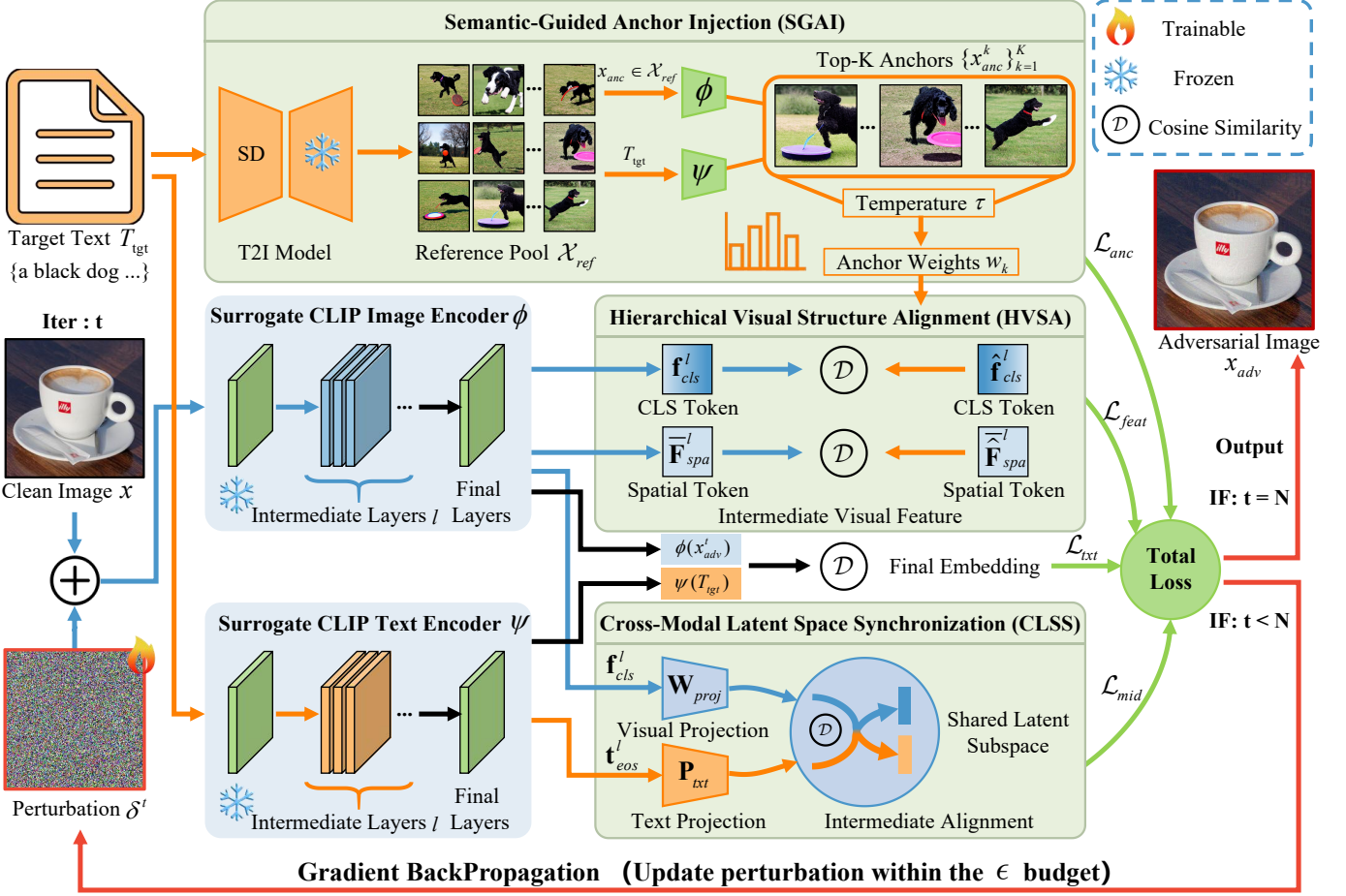


Fig. 2: Overview of the proposed SGHA-Attack framework for generating transferable targeted adversarial examples. The framework consists of three key components: SGAI, HVSA, and CLSS.

### III. METHODOLOGY

As illustrated in Fig. 2, we present SGHA-Attack, a transfer-based targeted attack framework designed to craft an adversarial example  $x_{adv}$  by injecting a human-imperceptible perturbation  $\delta$  into a clean image  $x$  (i.e.,  $x_{adv} = x + \delta$  subject to  $\|\delta\|_\infty \leq \epsilon$ ), aiming to mislead victim VLMs into generating attacker-specified outputs. The pipeline commences by constructing a visually grounded reference pool  $\mathcal{X}_{ref}$  via a frozen Text-to-Image (T2I) model conditioned on the target text  $T_{tgt}$ , from which the Top- $K$  most semantically relevant instances are adaptively selected as anchors. Subsequently, we perform iterative optimization on a CLIP surrogate, where the perturbation  $\delta$  is updated via gradient backpropagation to strictly align the hierarchical features of  $x_{adv}$  with these weighted anchor references while synchronizing visual and textual tokens across multiple depths, ultimately yielding the final transferable adversarial image. In the following subsections, we systematically elaborate on the three synergistic components that constitute this framework.

#### A. Semantic-Guided Anchor Injection

AttackVLM [13] shows that transfer-based targeted attacks can be driven by either text–image matching or image–image

matching on a surrogate model. For text–image matching, we align the surrogate embedding of the adversarial image with the target text embedding. Let  $\phi(\cdot)$  and  $\psi(\cdot)$  denote the surrogate image and text encoders, respectively, and define cosine distance as  $\mathcal{D}(\mathbf{a}, \mathbf{b}) = 1 - \cos(\mathbf{a}, \mathbf{b})$ . Here,  $\phi(\cdot)$  produces a global image embedding used for the following matching objectives. A standard objective is

$$\mathcal{L}_{txt} = \mathcal{D}(\phi(x_{adv}), \psi(T_{tgt})). \quad (1)$$

For image–image matching, the adversarial image is guided toward a reference image by matching their surrogate embeddings, which provides more visually grounded supervision. However, existing methods [13]–[16] often rely on a single reference instance, leading to narrow guidance: one image may capture only one appearance of the target concept, and the optimization can become sensitive to that particular target. This sensitivity makes targeted transfer less reliable when the victim model differs in backbone, alignment module, or processing pipeline.

To address this single-target limitation, we propose SGAI. Instead of using one target reference, SGAI constructs a set of semantic anchors that represent diverse visual realizations of the target concept, and uses them jointly as guidance via a weighted mixture. Concretely, we first build a reference pool

$\mathcal{X}_{ref}$  by sampling from a text-to-image generator conditioned on  $T_{tgt}$  (e.g., a diffusion model). Given the target text embedding  $\psi(T_{tgt})$ , we select the Top- $K$  anchors according to cosine similarity under the surrogate:

$$\{\mathbf{x}_{anc}^k\}_{k=1}^K = \text{TopK}_{\mathbf{x} \in \mathcal{X}_{ref}} \cos(\phi(\mathbf{x}), \psi(T_{tgt})). \quad (2)$$

We then compute importance weights using a temperature-scaled softmax:

$$w_k = \frac{\exp(\cos(\phi(\mathbf{x}_{anc}^k), \psi(T_{tgt}))/\tau)}{\sum_{j=1}^K \exp(\cos(\phi(\mathbf{x}_{anc}^j), \psi(T_{tgt}))/\tau)}. \quad (3)$$

Finally, we define an anchor-guided objective that aligns the adversarial embedding with a weighted mixture of anchor embeddings:

$$\mathcal{L}_{anc} = 1 - \sum_{k=1}^K w_k \cdot \cos(\phi(\mathbf{x}_{adv}), \phi(\mathbf{x}_{anc}^k)). \quad (4)$$

Compared with a single reference, the weighted anchor mixture provides richer and more stable guidance: different anchors cover different appearances of the same target concept, while the weights automatically emphasize the most relevant anchors. In practice, this reduces sensitivity to a single target and improves targeted transfer across diverse victim VLMs.

From an efficiency perspective, SGAI introduces limited overhead. Anchor features  $\phi(\mathbf{x}_{anc}^k)$  can be computed once and detached, and the iterative optimization only requires computing  $\phi(\mathbf{x}_{adv})$  each iteration. We report the runtime in Table VII.

### B. Hierarchical Visual Structure Alignment

SGAI provides a robust target guidance at the global embedding level, but many transfer-based attacks still impose constraints only on the final-layer embedding of the surrogate visual encoder. For ViT encoders, representations evolve progressively across layers: shallow layers capture low-level patterns, while deeper layers encode higher-level semantics. Consequently, restricting supervision to the final embedding may underutilize intermediate representations that influence transferability, especially when victim models vary in depth, patch size, or projector design. To address this, we propose HVSA, which aligns intermediate visual representations of  $\mathbf{x}_{adv}$  to anchor-derived targets at multiple layers.

Let  $\mathcal{L}$  denote a set of selected transformer layers. Denote by  $\phi^l(\cdot)$  the intermediate feature map extracted at layer  $l \in \mathcal{L}$ . Using the anchor weights  $\{w_k\}$  from Sec. III-A, we construct a layer-wise weighted anchor target:

$$\hat{\mathbf{F}}_{anc}^l = \sum_{k=1}^K w_k \cdot \phi^l(\mathbf{x}_{anc}^k). \quad (5)$$

This anchor-derived target provides a clear intermediate-layer reference based on the anchor images, making the supervision at each layer well-defined.

We further distinguish the roles of different ViT tokens. Let  $\mathbf{F}_{adv}^l = \phi^l(\mathbf{x}_{adv}) \in \mathbb{R}^{(N+1) \times D}$  be the feature map at layer  $l$ , where the first token corresponds to CLS and the remaining  $N$  tokens correspond to spatial patches. We decompose  $\mathbf{F}_{adv}^l$  and

$\hat{\mathbf{F}}_{anc}^l$  into global tokens  $(\mathbf{f}_{cls}^l, \hat{\mathbf{f}}_{cls}^l) \in \mathbb{R}^D$  and spatial tokens  $(\mathbf{F}_{spa}^l, \hat{\mathbf{F}}_{spa}^l) \in \mathbb{R}^{N \times D}$ . We mean-pool patch tokens to obtain a single spatial descriptor per layer:  $\bar{\mathbf{F}}_{spa}^l = \frac{1}{N} \sum_{i=1}^N \mathbf{F}_{spa}^l[i]$  (and similarly for  $\bar{\hat{\mathbf{F}}}_{spa}^l$ ). Mean pooling provides a compact spatial summary without requiring strict patch-to-patch correspondence, making the alignment more robust to differences in patch size and common preprocessing (e.g., resizing or cropping) across models. The HVSA loss is then defined as:

$$\mathcal{L}_{feat} = \sum_{l \in \mathcal{L}} \left( \lambda_{cls} \mathcal{D}(\mathbf{f}_{cls}^l, \hat{\mathbf{f}}_{cls}^l) + \lambda_{spa} \mathcal{D}(\bar{\mathbf{F}}_{spa}^l, \bar{\hat{\mathbf{F}}}_{spa}^l) \right). \quad (6)$$

The term weighted by  $\lambda_{cls}$  aligns the CLS token, encouraging the adversarial example to match the target at a global, image-level semantics across selected layers. The term weighted by  $\lambda_{spa}$  aligns the pooled patch tokens, encouraging consistency in spatial cues related to the target. We separate these two terms to provide complementary supervision: the CLS term focuses on global semantics, while the spatial term preserves coarse spatial cues, leading to a more balanced alignment signal.

### C. Cross-Modal Latent Space Synchronization

SGAI and HVSA mainly constrain the visual stream: SGAI provides target-guided anchors, and HVSA aligns intermediate visual features to anchor-derived targets across layers. However, a VLM produces outputs based on cross-modal interactions between vision and language. Thus, beyond final-layer matching, we enforce intermediate cross-modal alignment so that the intermediate visual features of  $\mathbf{x}_{adv}$  are aligned with the target text features.

A key challenge is that intermediate visual and textual features are not directly comparable before projection, since they may differ in dimension and representation space. To make them comparable, we map intermediate features into a shared latent subspace using projection heads available in the surrogate. For each layer  $l \in \mathcal{L}$ , we extract the intermediate CLS visual token  $\mathbf{f}_{cls}^l$  from the surrogate image encoder, and an intermediate text feature  $\mathbf{t}_{eos}^l$  from the surrogate text encoder, taken from the EOS token at the corresponding depth.

We then apply the visual and text projections and minimize the distance between them:

$$\mathcal{L}_{mid} = \sum_{l \in \mathcal{L}} \mathcal{D}(\mathbf{f}_{cls}^l \mathbf{W}_{proj}, \mathbf{t}_{eos}^l \mathbf{P}_{txt}), \quad (7)$$

where  $\mathbf{W}_{proj}$  and  $\mathbf{P}_{txt}$  are the surrogate's original visual and textual projection heads used for image-text alignment, mapping features into a shared latent subspace.

CLSS imposes cross-modal alignment at intermediate layers: after projection into the shared latent subspace, intermediate adversarial visual features are aligned with the target text features, instead of relying only on final-layer matching. During optimization,  $\mathcal{L}_{mid}$  provides cross-modal gradients at multiple depths, which improves targeted transfer when victim VLMs use different projection modules or cross-modal alignment schemes.

**Algorithm 1** The overall algorithm of SGHA-Attack

**Input:** Clean image  $x$ , target text  $T_{tgt}$ , text-to-image model T2I, surrogate image encoder  $\phi$ , text encoder  $\psi$ , visual projection  $\mathbf{W}_{proj}$ , text projection  $\mathbf{P}_{txt}$ , perturbation budget  $\epsilon$ , step size  $\alpha$ , steps  $N$ , layer set  $\mathcal{L}$ , weights  $\lambda_{anc}, \lambda_{feat}, \lambda_{cls}, \lambda_{spa}, \lambda_{mid}$ , temperature  $\tau$ .

**Output:** Adversarial image  $x_{adv}$ .

**Phase 1: Pre-processing**

- 1: Generate reference pool  $\mathcal{X}_{ref} \leftarrow \text{T2I}(T_{tgt})$
- 2: Select Top- $K$  anchors  $\{\mathbf{x}_{anc}^k\}_{k=1}^K \subset \mathcal{X}_{ref}$  by Eq. (2)
- 3: Compute anchor weights  $w_k$  via Eq. (3) with temperature  $\tau$ , forming a softmax mixture // SGAI
- 4: **for** each selected layer  $l \in \mathcal{L}$  **do**
  - // Extract weighted anchor features
  - 5:  $\hat{\mathbf{f}}_{cls}^l, \hat{\mathbf{F}}_{spa}^l \leftarrow \sum_{k=1}^K w_k \cdot \phi^l(\mathbf{x}_{anc}^k)$  // Extract target text features
  - 6:  $\mathbf{t}_{eos}^l \leftarrow \psi^l(T_{tgt})$
- 7: **end for**

**Phase 2: Adversarial Optimization**

- 8: Initialize perturbation  $\delta^0 \leftarrow \mathbf{0}$
- 9: **for**  $t = 0$  **to**  $N - 1$  **do**
- 10:  $\mathbf{x}_{adv}^t \leftarrow \mathbf{x} + \delta^t$
- 11:  $\mathcal{L}_{txt} \leftarrow \mathcal{D}(\phi(\mathbf{x}_{adv}^t), \psi(T_{tgt}))$  // Final embedding
- 12:  $\mathcal{L}_{anc} \leftarrow 1 - \sum_{k=1}^K w_k \cdot \cos(\phi(\mathbf{x}_{adv}^t), \phi(\mathbf{x}_{anc}^k))$
- 13:  $\mathcal{L}_{feat} \leftarrow 0, \mathcal{L}_{mid} \leftarrow 0$
- 14: **for** each selected layer  $l \in \mathcal{L}$  **do**
  - // Extract adversarial features
  - 15:  $\mathbf{f}_{cls}^l, \hat{\mathbf{F}}_{spa}^l \leftarrow \phi^l(\mathbf{x}_{adv}^t)$  // HVSA: Align intermediate visual features
  - 16:  $\mathcal{L}_{feat} \leftarrow \mathcal{L}_{feat} + \lambda_{cls} \mathcal{D}(\mathbf{f}_{cls}^l, \hat{\mathbf{f}}_{cls}^l) + \lambda_{spa} \mathcal{D}(\hat{\mathbf{F}}_{spa}^l, \hat{\mathbf{F}}_{spa}^l)$  // CLSS: Synchronize cross-modal features
  - 17:  $\mathcal{L}_{mid} \leftarrow \mathcal{L}_{mid} + \mathcal{D}(\mathbf{f}_{cls}^l \mathbf{W}_{proj}, \mathbf{t}_{eos}^l \mathbf{P}_{txt})$
- 18: **end for**
- 19:  $\mathcal{L}_{total} \leftarrow \mathcal{L}_{txt} + \lambda_{anc} \mathcal{L}_{anc} + \lambda_{feat} \mathcal{L}_{feat} + \lambda_{mid} \mathcal{L}_{mid}$
- 20:  $\mathbf{g}^t \leftarrow \nabla_{\mathbf{x}_{adv}^t} \mathcal{L}_{total}$  // Gradient backpropagation
- 21:  $\delta^{t+1} \leftarrow \text{Clip}_{[-\epsilon, \epsilon]}(\delta^t - \alpha \cdot \text{sign}(\mathbf{g}^t))$  // Update
- 22: **end for**
- 23:  $\mathbf{x}_{adv} \leftarrow \text{Clip}_{[-\epsilon, \epsilon]}(\mathbf{x} + \delta^N)$
- 24: **return**  $\mathbf{x}_{adv}$

**D. Total Objective and Optimization Procedure**

We integrate the three modules, SGAI, HVSA, and CLSS, into a unified objective function:

$$\mathcal{L}_{total} = \mathcal{L}_{txt} + \lambda_{anc} \mathcal{L}_{anc} + \lambda_{feat} \mathcal{L}_{feat} + \lambda_{mid} \mathcal{L}_{mid}, \quad (8)$$

where  $\lambda_{anc}$ ,  $\lambda_{feat}$ , and  $\lambda_{mid}$  balance anchor guidance, hierarchical visual alignment, and intermediate cross-modal synchronization. We optimize  $\mathbf{x}_{adv}$  using projected gradient descent under an  $\ell_\infty$  budget  $\epsilon$ . At each iteration, the adversarial image is updated using the sign of the gradient and projected back to the feasible  $\ell_\infty$  ball around  $\mathbf{x}$ , pixel values are also clipped to the valid range. Algorithm 1 summarizes the complete procedure.

**TABLE I:** Configurations of the victim VLMs.

Category	Model	Params	Vision Module	Text Module / LLM
Open-Source	UniDiffuser [47]	1.4B	CLIP ViT-B/32	UVIT-H (Diffusion)
	BLIP-2 [28]	12.1B	ViT-G/14 (EVA-CLIP)	FLAN-T5 XXL
	InstructBLIP [29]	14.2B	ViT-G/14 (EVA-CLIP)	Vicuna-13B
	MiniGPT-4 [27]	14.2B	ViT-G/14 (EVA-CLIP)	Vicuna-13B
	LLaVA [3]	13.3B	CLIP ViT-L/14	Vicuna-13B
	LLaVA-NeXT [48]	72.3B	CLIP ViT-L/14-336px	Qwen1.5-72B-Chat
Closed-Source	OpenAI GPT-4o		Undisclosed	
	Google Gemini-2.0		Undisclosed	
	Anthropic Claude-3.5		Undisclosed	

**IV. EXPERIMENTS**
**A. Experimental Settings**

**Datasets.** We follow the evaluation protocol in [13], [14]. Specifically, we sample 1,000 images from ImageNet-1K [44] as clean inputs and sample 1,000 text descriptions from MS-COCO [45] as target prompts. Each ImageNet image is randomly paired with one MS-COCO description, which typically yields a semantic mismatch between the source image and the target text, forming a challenging targeted setting. Following [13], we further use Stable Diffusion [46] to synthesize text-conditioned target reference images from the target descriptions.

**Victim VLMs.** We select a diverse set of victim models to evaluate the effectiveness of our attack, including six state-of-the-art open-source VLMs and three leading closed-source commercial models. The detailed configurations are summarized in Table I. It is worth noting that certain models (e.g., MiniGPT-4 and InstructBLIP) share identical vision backbones and parameter scales but employ distinct cross-modal alignment mechanisms (e.g., linear projection vs. Q-Former), thereby serving as diverse testbeds for evaluating transferability. Regarding the black-box attack setting, we follow the attack protocols in [13] and [15] for open-source and closed-source commercial models, respectively.

**Baselines.** We benchmark against state-of-the-art transfer-based targeted attacks categorized into two groups: VLM-specific approaches, including MF-it [13], MF-ii [13], COA [14], AdvDiffVLM [16], and M-Attack [15]. Following [16], we also adapt representative SOTA image classification methods BSR [49] and OPS [32] for the VLM task by replacing their classification loss with a target-embedding alignment loss.

**Evaluation metrics.** Following standard protocols [13], [14], we employ CLIP-Score [13] to measure semantic consistency and the LLM-based (GPT-4) Attack Success Rate (ASR) [14] to assess effectiveness, specifically utilizing  $\text{ASR}_{\text{fool}}$  for untargeted attack success and  $\text{ASR}_{\text{target}}$  for targeted attack success. Additionally, we utilize Structural Similarity (SSIM) [50] and Peak Signal-to-Noise Ratio (PSNR) to evaluate the visual imperceptibility of the generated adversarial examples.

**Implementation Details.**<sup>1</sup> We utilize PGD [51] with a maximum perturbation of  $\epsilon = 8/255$  and 100 iterations under the  $L_\infty$  norm across all methods to ensure fair comparison. For SGHA-Attack, we set anchor parameters to  $K = 5$ ,  $\tau = 5$ , and  $\lambda_{anc} = 1$ . To determine the intermediate layers  $\mathcal{L}$ , we adopt a

<sup>1</sup>Code available at: <https://github.com/BiiiGerrr/SGHA-Attack>

TABLE II: Quantitative comparison of transfer-based targeted attacks against black-box VLMs. We report the CLIP Score ( $\uparrow$ ) to measure semantic consistency across various text encoders and their ensemble average, alongside the LLM-based ASR evaluated by GPT-4. In the following tables, highlighted, underlined, and gray-shaded values indicate the best, second-best, and our method’s results, respectively, for each case.

VLM Model	Attack Method	Text Encoder for Evaluation (CLIP Score $\uparrow$ )						ASR ( $\uparrow$ )	
		RN50	RN101	ViT-B/16	ViT-B/32	ViT-B/14	Ensemble	ASR <sub>fool</sub>	ASR <sub>target</sub>
UniDiffuser [47]	Clean Image	0.4417	0.4275	0.4504	0.4690	0.3215	0.4220	0.00%	0.00%
	BSR [49]	0.5415	0.5244	0.5542	0.5728	0.4382	0.5262	72.30%	18.00%
	OPS [32]	0.6470	0.6284	0.6592	0.6748	0.5635	0.6345	94.40%	52.30%
	M-Attack [15]	0.5620	0.5454	0.5747	0.5908	0.4617	0.5469	73.30%	23.10%
	AdvDiffVLM [16]	0.6465	0.6289	0.6582	0.6748	0.5630	0.6343	90.20%	51.90%
	MF-it [13]	0.6768	0.6577	0.6909	0.7065	0.5933	0.6650	91.10%	48.20%
	MF-ii [13]	0.7061	0.6929	0.7188	0.7324	0.6353	0.6970	98.00%	72.10%
	COA [14]	0.7100	0.6880	0.7217	0.7398	0.6284	0.6976	98.80%	73.20%
BLIP2 [28]	<b>Ours</b>	<b>0.7793</b>	<b>0.7647</b>	<b>0.7891</b>	<b>0.7998</b>	<b>0.7197</b>	<b>0.7705</b>	<b>99.80%</b>	<b>89.40%</b>
	Clean Image	0.4663	0.4526	0.4763	0.4954	0.3491	0.4480	0.00%	0.00%
	BSR [49]	0.5874	0.5659	0.5991	0.6162	0.4858	0.5709	55.00%	20.80%
	OPS [32]	0.6475	0.6255	0.6582	0.6743	0.5581	0.6327	72.10%	34.80%
	M-Attack [15]	0.5376	0.5161	0.5498	0.5669	0.4292	0.5199	30.80%	9.90%
	AdvDiffVLM [16]	0.6333	0.6133	0.6450	0.6616	0.5440	0.6194	63.70%	32.90%
	MF-it [13]	0.7607	0.7446	0.7715	0.7813	0.6943	0.7505	93.50%	70.60%
	MF-ii [13]	0.7676	0.7529	0.7773	0.7896	0.7041	0.7583	97.80%	82.80%
InstructBLIP [29]	COA [14]	0.7754	0.7598	0.7852	0.7959	0.7110	0.7654	99.30%	80.20%
	<b>Ours</b>	<b>0.8359</b>	<b>0.8228</b>	<b>0.8438</b>	<b>0.8525</b>	<b>0.7861</b>	<b>0.8282</b>	<b>99.40%</b>	<b>94.70%</b>
	Clean Image	0.4639	0.4544	0.4756	0.4934	0.3442	0.4463	0.00%	0.00%
	BSR [49]	0.5801	0.5635	0.5903	0.6060	0.4775	0.5635	55.20%	22.00%
	OPS [32]	0.6367	0.6196	0.6484	0.6626	0.5444	0.6224	71.70%	34.10%
	M-Attack [15]	0.5337	0.5161	0.5435	0.5601	0.4209	0.5148	32.00%	9.30%
	AdvDiffVLM [16]	0.6333	0.6167	0.6455	0.6587	0.5405	0.6189	66.80%	35.20%
	MF-it [13]	0.7603	0.7456	0.7700	0.7803	0.6948	0.7502	94.10%	73.70%
MiniGPT-4 [27]	MF-ii [13]	0.7695	0.7544	0.7783	0.7886	0.7036	0.7589	98.40%	84.00%
	COA [14]	0.7720	0.7583	0.7832	0.7920	0.7075	0.7626	99.10%	81.30%
	<b>Ours</b>	<b>0.8345</b>	<b>0.8223</b>	<b>0.8423</b>	<b>0.8501</b>	<b>0.7827</b>	<b>0.8264</b>	<b>99.30%</b>	<b>95.70%</b>
	Clean Image	0.2871	0.3916	0.3252	0.3569	0.2131	0.3148	0.00%	0.00%
	BSR [49]	0.3696	0.4873	0.4229	0.4458	0.3196	0.4090	55.20%	20.30%
	OPS [32]	0.3945	0.5288	0.4536	0.4724	0.3596	0.4418	71.80%	35.60%
	M-Attack [15]	0.3311	0.4446	0.3792	0.4063	0.2703	0.3663	29.90%	7.90%
	AdvDiffVLM [16]	0.3982	0.5269	0.4561	0.4773	0.3630	0.4443	63.70%	31.50%
LLaVA [3]	MF-it [13]	0.4929	0.6270	0.5591	0.5737	0.4793	0.5464	94.60%	72.00%
	MF-ii [13]	0.5112	0.6431	0.5781	0.5898	0.4998	0.5644	98.10%	81.00%
	COA [14]	0.5161	0.6445	0.5850	0.5962	0.5054	0.5694	99.60%	78.70%
	<b>Ours</b>	<b>0.5850</b>	<b>0.7061</b>	<b>0.6519</b>	<b>0.6602</b>	<b>0.5801</b>	<b>0.6366</b>	<b>99.70%</b>	<b>95.60%</b>
	Clean Image	0.3413	0.4395	0.3770	0.4021	0.2341	0.3588	0.00%	0.00%
	BSR [49]	0.4734	0.5444	0.5171	0.5308	0.3901	0.4912	64.80%	25.30%
	OPS [32]	0.5064	0.5767	0.5503	0.5635	0.4277	0.5249	72.50%	39.70%
	M-Attack [15]	0.4233	0.5015	0.4609	0.4802	0.3252	0.4382	40.40%	11.10%
LLaVA-NeXT [48]	AdvDiffVLM [16]	0.4800	0.5513	0.5205	0.5396	0.3945	0.4972	60.70%	25.40%
	MF-it [13]	0.4922	0.5640	0.5366	0.5523	0.4209	0.5132	67.70%	27.60%
	MF-ii [13]	0.5625	0.6274	0.6128	0.6211	0.5000	0.5848	88.00%	61.00%
	COA [14]	0.5200	0.5913	0.5679	0.5786	0.4495	0.5415	88.90%	42.40%
	<b>Ours</b>	<b>0.6821</b>	<b>0.7246</b>	<b>0.7358</b>	<b>0.7324</b>	<b>0.6460</b>	<b>0.7042</b>	<b>99.10%</b>	<b>96.40%</b>
	Clean Image	0.2673	0.3809	0.3054	0.3120	0.1897	0.2911	0.00%	0.00%
	BSR [49]	0.3723	0.4729	0.4143	0.4097	0.2869	0.3912	56.50%	14.80%
	OPS [32]	0.3662	0.4727	0.4067	0.4019	0.2791	0.3853	53.60%	14.90%
LLaVA-NeXT [48]	M-Attack [15]	0.3181	0.4268	0.3567	0.3562	0.2300	0.3375	29.80%	4.40%
	AdvDiffVLM [16]	0.3306	0.4382	0.3706	0.3713	0.2441	0.3510	37.90%	5.80%
	MF-it [13]	0.3325	0.4377	0.3674	0.3711	0.2417	0.3501	33.70%	4.10%
	MF-ii [13]	0.3738	0.4780	0.4104	0.4104	0.2874	0.3920	49.90%	15.60%
	COA [14]	0.3650	0.4648	0.4031	0.4019	0.2703	0.3810	60.30%	10.60%
	<b>Ours</b>	<b>0.5391</b>	<b>0.6338</b>	<b>0.5869</b>	<b>0.5835</b>	<b>0.4944</b>	<b>0.5675</b>	<b>92.60%</b>	<b>73.40%</b>

Deep-Layer Uniform Sampling strategy, specifically selecting layers  $\{7, 9, 11\}$  for the base ViT-B/32 model. The balancing weights  $\{\lambda_{feat}, \lambda_{cls}, \lambda_{spa}, \lambda_{mid}\}$  are scaled according to the backbone architecture, for instance, they are set to 1.5, 1.0, 0.7, 2.5 for ViT-B/32. For larger models like ViT-L and ViT-G, we proportionally increase the feature alignment weights and apply the corresponding layer mappings to accommodate their higher-dimensional feature spaces and deeper architectures.

### B. Comprehensive Evaluation on Open-Source VLMs

In this section, we present a comprehensive evaluation of our proposed method against state-of-the-art transfer-based

targeted attacks. We conduct experiments across six representative open-source VLMs ranging from 1.4B to 72.3B parameters, including UniDiffuser, BLIP-2, InstructBLIP, MiniGPT-4, LLaVA, and LLaVA-NeXT. To ensure a consistent evaluation setting, we employ a unified prompt: “*What is the content of the image?*” during the inference phase.

**Quantitative Attack Performance.** We first conduct a quantitative comparison to assess the attack effectiveness. As reported in Table II, our method demonstrates superior performance across all metrics.

- 1) Our method consistently achieves state-of-the-art performance in both ASR<sub>fool</sub> and ASR<sub>target</sub> metrics across

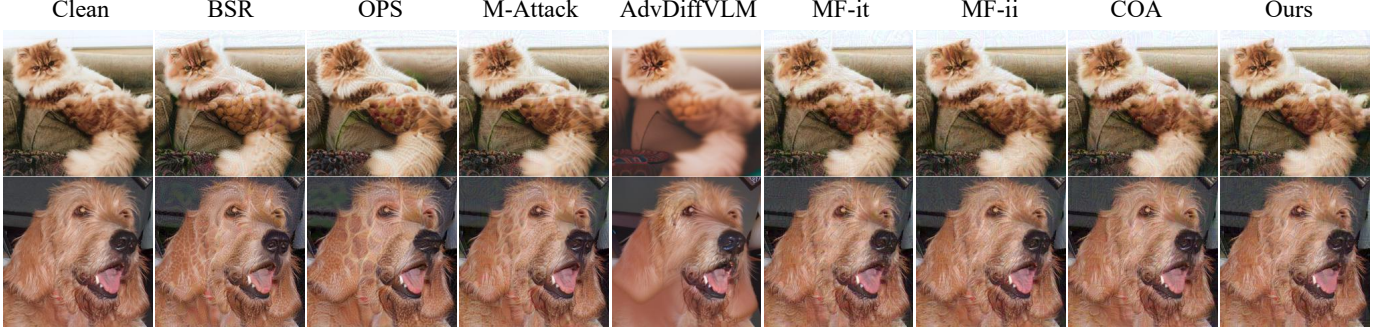


Fig. 3: Visual comparison of adversarial examples generated by various attack methods.

all evaluated models. Specifically, regarding the challenging ASR<sub>target</sub> which measures the targeted semantic accuracy, SGHA-Attack demonstrates substantial improvements over the strongest baselines. For instance, on the 12.1B parameter BLIP-2 model, we achieve an ASR<sub>target</sub> of 94.70%, significantly surpassing MF-ii (82.80%) and COA (80.20%). This indicates that our approach not only successfully misleads the VLMs but also precisely steers them toward the target semantics, reducing irrelevant outputs.

- 2) In terms of semantic consistency, our approach yields significant gains in Ensemble CLIP Scores. High CLIP scores imply that the generated adversarial captions are semantically aligned with the target prompts across diverse vision encoders. As shown in Table II, SGHA-Attack obtains the highest scores on all six victim models (e.g., 0.8282 on BLIP-2 compared to 0.7654 for COA). This confirms that our hierarchical alignment generates generalizable semantic features rather than overfitting to surrogate-specific biases and artifacts, ensuring the adversarial perturbations remain effective across different feature extractors.
- 3) Regarding robustness across model scales and architectures, our method exhibits strong generalization from the lightweight 1.4B UniDiffuser to the 72.3B LLaVA-NeXT. Regardless of the underlying cross-modal alignment mechanisms (e.g., linear projection or Q-Former), our attack maintains high efficacy. Notably, on LLaVA-NeXT where standard methods struggle due to stronger robustness, SGHA-Attack maintains a high success rate of 73.40%. This validates that our multi-granularity strategy effectively generalizes across architectures defenses to establish robust semantic control.

**Visual Quality Performance.** We evaluate the visual quality and targeted effectiveness of the generated adversarial examples through both quantitative metrics reported in Table III and qualitative visualizations presented in Fig. 3 and Fig. 4.

- 1) As shown in Table III, performance varies significantly by attack category. Unrestricted methods like AdvDiffVLM suffer from noticeable structural degradation (SSIM 0.69) due to their diffusion-based generation process. In contrast, perturbation-constrained methods operate under a standard budget ( $\epsilon = 8/255$ ) and consistently

TABLE III: Quantitative evaluation of visual quality.

Category	Method	SSIM $\uparrow$	PSNR $\uparrow$
Unrestricted	AdvDiffVLM [16]	0.69	23.06
Perturbation Constrained	BSR [49]	0.83	31.65
	OPS [32]	0.83	31.26
	M-Attack [15]	0.89	33.78
	MF-it [13]	0.89	33.98
	MF-ii [13]	0.90	34.28
	COA [14]	0.89	33.68
<b>Ours</b>		<b>0.89</b>	33.71

maintain high structural integrity. Our method achieves an SSIM of 0.89 and PSNR of 33.71, demonstrating that our approach yields visual quality comparable to state-of-the-art constrained baselines (e.g., MF-ii) while significantly surpassing unrestricted approaches. This imperceptibility is qualitatively supported by Fig. 3, while unrestricted approaches introduce observable blurring artifacts, our method produces perturbations that are virtually imperceptible to the human eye, preserving texture details and color consistency.

- 2) We further demonstrate the practical effectiveness of these attacks in Fig. 4. Despite keeping the perturbation nearly imperceptible, our method can reliably steer the model’s interpretation toward the target semantics. For instance, in Fig. 4(a), although the image clearly shows “three white wolves”, UniDiffuser is induced to describe it as a “bathroom with tiled walls”. Even for the more robust LLaVA-NeXT (Fig. 4(f)), our method drives the model to generate “laptop computers” from an image of a salamander. These examples show that our approach achieves precise targeted control by enforcing target-aligned semantics, causing the model’s generated descriptions to follow the target prompt rather than the original visual content.

### C. Evaluation on Closed-Source Commercial VLMs

In this section, we assess the practical threat of our method in real-world black-box scenarios by extending our evaluation to three leading commercial VLMs: OpenAI GPT-4o, Google Gemini-2.0, and Anthropic Claude-3.5. Due to the high inference costs and rate limits associated with commercial APIs, we

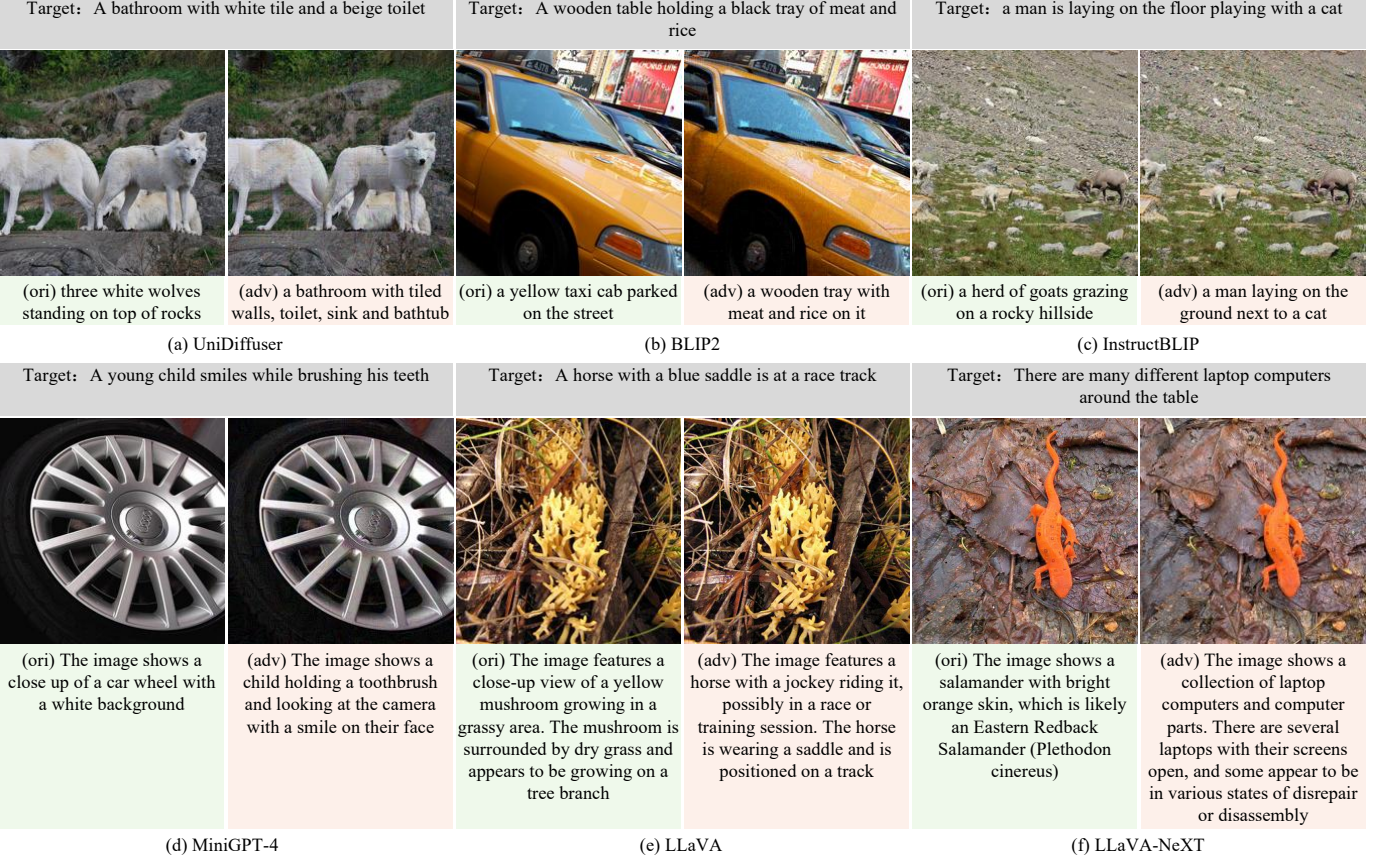


Fig. 4: Qualitative results of our attack on multiple open-source VLMs. The target text prompt is shown above each image pair. For each example, the left image is the clean original with its caption, and the right image is the adversarial example generated by our method ( $\epsilon = 8/255$ ) with the model-generated caption. The adversarial captions closely align with the target texts, while the images remain visually similar to the originals.

conduct this evaluation on a subset of 100 randomly sampled image-text pairs. To ensure a fair and rigorous assessment against these strongly aligned models, we adopt the experimental protocols established in M-Attack [15], utilizing an ensemble of three CLIP visual encoders as surrogates.

**Quantitative Attack Performance.** We report the quantitative performance in Table IV, covering both standard ( $\epsilon = 8/255$ ) and enhanced ( $\epsilon = 16/255$ ) perturbation settings to demonstrate performance gains when integrating our strategy into the M-Attack framework.

- 1) Our method exhibits stronger effectiveness in both breaking model recognition ( $ASR_{fool}$ ) and achieving targeted semantics ( $ASR_{target}$ ). Under the “Enhanced Setting” ( $\epsilon = 16/255$ ), we achieve a 97%  $ASR_{fool}$  on GPT-4o (vs. 87% for M-Attack), demonstrating our ability to reliably disrupt the model’s visual understanding. More importantly, we translate this disruption into targeted control, boosting  $ASR_{target}$  from 47% to 79%. This superiority extends to the robust Claude-3.5, where we surpass M-Attack in both fooling rate (67% vs 52%) and targeted success (26% vs 7%). Notably, our constrained attack even outperforms the unrestricted AdvDiffVLM (12% success on GPT-4o) significantly, highlighting the efficiency of our semantic-guided optimization.

- 2) Beyond success rates, our method consistently achieves the highest Ensemble CLIP Scores, supporting the generality of the learned hierarchical semantic alignment. For instance, under the Enhanced setting for GPT-4o, we reach an Ensemble Score of 0.6098, surpassing M-Attack (0.5714). This confirms that our hierarchical alignment ensures the target semantics are robustly recognized across diverse visual encoders, rather than overfitting to a specific surrogate.

**Visual Quality Performance.** We further provide visual evidence and imperceptibility analysis based on Figure 5 and the visual metrics in Table IV.

- 1) As shown in the Visual Metrics column of Table IV, our method maintains high structural integrity. Under the standard setting, we achieve an SSIM of 0.89 comparable to the clean baseline. Even in the enhanced setting, our method (SSIM 0.75) preserves significantly better visual quality than the unrestricted AdvDiffVLM (SSIM 0.69), which suffers from severe distortions. This quantitatively demonstrates that our method avoids the blurring artifacts typical of diffusion-based attacks while delivering stronger transferability.
- 2) Figure 5 provides qualitative evidence of our attack’s precision. We successfully decouple semantic interpreta-

TABLE IV: Quantitative performance comparison on commercial black-box VLMs. We compare methods under Standard ( $\epsilon = 8/255$ ), Unrestricted, and Enhanced ( $\epsilon = 16/255$ ) settings. Ens. denotes the Ensemble CLIP Score.

Setting	Method	Visual Metrics		GPT-4o			Gemini-2.0			Claude-3.5		
		SSIM	PSNR	Ens.	ASR <sub>fool</sub>	ASR <sub>target</sub>	Ens.	ASR <sub>fool</sub>	ASR <sub>target</sub>	Ens.	ASR <sub>fool</sub>	ASR <sub>target</sub>
<b>Clean</b>	No Attack	1.00	Inf	0.3078	0%	0%	0.2345	0%	0%	0.2558	0%	0%
<b>Standard</b> 100 iter $\epsilon = 8/255$	MF-ii [13]	<b>0.90</b>	<b>34.32</b>	0.3559	8%	0%	0.3651	7%	0%	0.2812	12%	0%
	M-Attack [15]	0.89	33.82	0.4166	32%	4%	0.4096	25%	3%	0.2913	19%	1%
	<b>Ours</b>	0.89	33.71	0.4699	61%	20%	0.4466	37%	8%	0.3120	25%	3%
<b>Unrestricted</b>	AdvDiffVLM [16]	0.69	23.41	0.5101	61%	12%	0.4853	46%	8%	0.3466	41%	9%
<b>Enhanced</b> 300 iter $\epsilon = 16/255$	MF-ii [13]	0.74	28.79	0.3759	14%	0%	0.3715	9%	0%	0.2874	19%	0%
	M-Attack [15]	0.75	28.79	0.5714	87%	47%	0.5516	79%	45%	0.3502	52%	7%
	<b>Ours</b>	0.75	28.73	<b>0.6098</b>	<b>97%</b>	<b>79%</b>	<b>0.6104</b>	<b>89%</b>	<b>67%</b>	<b>0.4065</b>	<b>67%</b>	<b>26%</b>

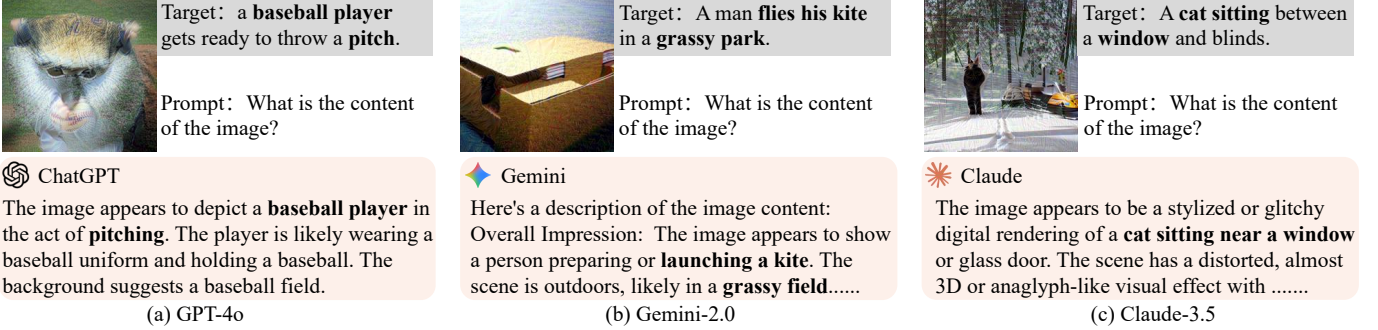


Fig. 5: Visualization of targeted adversarial attacks on commercial black-box VLMs. We display the adversarial image, the target text, and the actual response generated by the model.

tion from visual content without arousing suspicion. For instance, in Figure 5(a), GPT-4o incorrectly describes a monkey as a “baseball player” preparing to pitch. Similarly, Gemini-2.0 describes a box as a person “launching a kite”, and Claude-3.5 perceives a “cat sitting” near a window. These examples confirm that our method can induce targeted descriptions while preserving the visual realism of the original images.

#### D. Robustness Against Adversarial Defenses

To evaluate robustness against preprocessing-based defenses, we test our method against Bit Reduction (4-bit) [52], JPEG Compression (QF=75) [53], ComDefend [54], and DiffPure [55]. As shown in Table V, our method consistently outperforms baselines in maintaining high ASR<sub>target</sub> and Ensemble CLIP Scores. Notably, under quantization and compression, our method significantly surpasses both MF-ii and COA across all victim models. This robustness indicates that our hierarchical alignment strategy encourages robust target-aligned representations features into the deep semantic structure of the image, allowing target semantics to survive input transformations and signal purification mechanisms that typically filter out superficial perturbations.

In comparison, while COA exhibits comparable fooling rates, its performance in targeted attacks decreases markedly under defense mechanisms. We attribute this to COA’s reliance on high-frequency priors from an auxiliary network, which tends to yield high-frequency noise patterns. While effective

at disrupting recognition (high ASR<sub>fool</sub>), these patterns are less robust semantically and are easily smoothed out by purification. In contrast, our method focuses on semantic robustness through cross-modal synchronization. By constructing a robust semantic skeleton rather than relying on fragile noise, our adversarial features remain effective even after purification, yielding significantly higher targeted attack success rates compared to COA across diverse defense settings.

#### E. Ablation of the Three Proposed Modules

We conduct ablation studies on UniDiffuser, BLIP-2, and LLaVA to examine the contribution of each component. We use MF-it as the baseline, which optimizes  $\mathcal{L}_{txt}$  only. As shown in Table VI, enabling SGAI, HVSA, and CLSS corresponds to adding  $\mathcal{L}_{anc}$ ,  $\mathcal{L}_{feat}$ , and  $\mathcal{L}_{mid}$ , respectively, and the full model uses all three terms together with  $\mathcal{L}_{txt}$ .

Overall, adding any single component on top of MF-it consistently improves targeted control and semantic consistency. In particular, introducing SGAI ( $+\mathcal{L}_{anc}$ ) yields a large gain across all three models, e.g., on LLaVA, ASR<sub>target</sub> increases from 27.60% to 66.10%. HVSA ( $+\mathcal{L}_{feat}$ ) provides the strongest boost on the challenging instruction-tuned model, raising ASR<sub>target</sub> on LLaVA to 92.90%, and combining SGAI and HVSA further improves it to 96.20%. CLSS ( $+\mathcal{L}_{mid}$ ) offers complementary cross-modal guidance, improving the overall balance of Ensemble CLIP Score and targeted success when combined with the other terms. Finally, the full objective achieves the best overall performance across models,

TABLE V: Defense-aware black-box attacks against victim VLMs. We evaluate Ens.,  $\text{ASR}_{\text{fool}}$ , and  $\text{ASR}_{\text{target}}$  under four preprocessing-based defenses: Bit Reduction, JPEG Compression, ComDefend, and DiffPure.

VLM Model	Attack	Bit Reduction [52]			JPEG Compression [53]			ComDefend [54]			DiffPure [55]		
		Ens.	$\text{ASR}_{\text{fool}}$	$\text{ASR}_{\text{target}}$	Ens.	$\text{ASR}_{\text{fool}}$	$\text{ASR}_{\text{target}}$	Ens.	$\text{ASR}_{\text{fool}}$	$\text{ASR}_{\text{target}}$	Ens.	$\text{ASR}_{\text{fool}}$	$\text{ASR}_{\text{target}}$
UniDiffuser	AdvDiffVLM [16]	0.5422	69.20%	21.60%	0.5497	72.20%	24.00%	0.4900	62.50%	10.50%	0.5110	62.80%	14.40%
	MF-ii [13]	0.6599	94.40%	60.00%	0.6316	91.30%	51.20%	0.5611	79.10%	28.70%	0.5061	56.00%	13.20%
	COA [14]	0.6833	<b>98.40%</b>	<b>65.60%</b>	0.6551	<b>98.40%</b>	<b>56.80%</b>	0.5823	<b>93.30%</b>	<b>34.50%</b>	0.5447	<b>83.40%</b>	<b>20.30%</b>
	<b>Ours</b>	<b>0.7452</b>	<b>97.30%</b>	<b>81.70%</b>	<b>0.7225</b>	<b>97.10%</b>	<b>77.10%</b>	<b>0.6505</b>	<b>91.00%</b>	<b>56.00%</b>	<b>0.5686</b>	<b>70.10%</b>	<b>27.20%</b>
BLIP-2	AdvDiffVLM [16]	0.5675	45.90%	19.60%	0.5281	42.50%	11.90%	0.5098	32.30%	8.10%	0.5512	41.50%	<u>13.70%</u>
	MF-ii [13]	0.6532	75.50%	42.60%	0.5169	37.40%	12.40%	0.5095	31.40%	9.00%	0.5158	27.40%	7.10%
	COA [14]	0.6912	<u>90.50%</u>	<u>56.40%</u>	0.5446	<b>60.20%</b>	<u>15.60%</u>	0.5413	<b>55.60%</b>	<u>14.40%</u>	0.5337	<b>48.00%</b>	11.60%
	<b>Ours</b>	<b>0.7575</b>	<b>91.90%</b>	<b>73.90%</b>	<b>0.5882</b>	56.40%	<b>27.40%</b>	<b>0.5738</b>	<u>51.80%</u>	<b>24.30%</b>	<b>0.5600</b>	<u>43.30%</u>	<b>18.50%</b>
InstructBLIP	AdvDiffVLM [16]	0.5645	48.70%	19.30%	0.5123	38.70%	11.50%	0.5173	34.30%	8.90%	0.5453	43.00%	<u>15.00%</u>
	MF-ii [13]	0.6412	77.00%	43.50%	0.5098	33.70%	10.60%	0.5161	32.80%	9.70%	0.5126	27.40%	7.60%
	COA [14]	0.6830	<u>92.20%</u>	<u>56.00%</u>	0.5403	<b>59.30%</b>	<u>15.70%</u>	0.5420	<b>55.50%</b>	<u>14.60%</u>	0.5318	<b>47.80%</b>	11.60%
	<b>Ours</b>	<b>0.7484</b>	<b>93.30%</b>	<b>74.40%</b>	<b>0.5747</b>	54.00%	<b>25.10%</b>	<b>0.5766</b>	<u>51.70%</u>	<b>23.30%</b>	<b>0.5610</b>	<u>44.90%</u>	<b>18.20%</b>
MiniGPT-4	AdvDiffVLM [16]	0.3901	44.70%	15.80%	0.3813	38.80%	9.80%	0.3833	31.40%	6.00%	0.3899	38.50%	<u>10.80%</u>
	MF-ii [13]	0.4547	76.30%	39.30%	0.3776	35.50%	8.90%	0.3970	31.10%	7.30%	0.3759	25.00%	6.40%
	COA [14]	0.4946	<u>92.70%</u>	<u>52.80%</u>	0.3991	<b>62.60%</b>	<u>14.10%</u>	0.4213	<b>57.60%</b>	<u>13.00%</u>	0.3910	<b>48.80%</b>	9.50%
	<b>Ours</b>	<b>0.5574</b>	<b>93.90%</b>	<b>73.40%</b>	<b>0.4325</b>	54.70%	<b>24.20%</b>	<b>0.4498</b>	<u>50.30%</u>	<b>22.40%</b>	<b>0.4202</b>	<u>42.50%</u>	<b>16.20%</b>
LLaVA	AdvDiffVLM [16]	0.4247	34.00%	6.60%	0.4313	34.40%	6.80%	0.4054	26.10%	2.10%	0.4248	31.60%	5.20%
	MF-ii [13]	0.5160	66.20%	<u>30.30%</u>	0.4450	39.40%	<u>11.40%</u>	0.4063	24.50%	4.40%	0.4131	18.10%	2.60%
	COA [14]	0.4986	<u>76.70%</u>	23.20%	0.4137	40.60%	3.80%	0.4104	35.10%	2.60%	0.4437	<b>41.60%</b>	<u>10.80%</u>
	<b>Ours</b>	<b>0.6402</b>	<b>93.50%</b>	<b>76.40%</b>	<b>0.5380</b>	<b>70.10%</b>	<b>38.10%</b>	<b>0.4710</b>	<b>46.20%</b>	<b>18.00%</b>	<b>0.4520</b>	<u>37.40%</u>	<b>11.90%</b>
LLaVA-NeXT	AdvDiffVLM [16]	0.3413	27.40%	1.30%	0.3267	26.90%	1.90%	0.3417	27.70%	0.40%	0.3294	24.80%	1.20%
	MF-ii	0.3301	39.50%	<u>9.50%</u>	0.3622	26.50%	<u>3.50%</u>	0.3276	20.90%	<u>1.30%</u>	0.3172	15.20%	0.80%
	COA [14]	0.3701	58.50%	6.10%	0.3326	32.60%	1.70%	0.3358	31.90%	1.00%	0.3375	<b>30.20%</b>	3.30%
	<b>Ours</b>	<b>0.4843</b>	<b>78.50%</b>	<b>44.40%</b>	<b>0.3954</b>	<b>49.20%</b>	<b>15.80%</b>	<b>0.3660</b>	<b>37.50%</b>	<b>7.40%</b>	<b>0.3423</b>	<u>25.60%</u>	<b>3.80%</b>

TABLE VI: Ablation of the three proposed modules (SGAI, HVSA, and CLSS). We report Ens.,  $\text{ASR}_{\text{fool}}$ , and  $\text{ASR}_{\text{target}}$  on multiple VLMs.  $\mathcal{L}_{\text{txt}}$  is the baseline, adding  $\mathcal{L}_{\text{anc}}$ ,  $\mathcal{L}_{\text{feat}}$ , and  $\mathcal{L}_{\text{mid}}$  activates SGAI, HVSA, and CLSS, respectively.

$\mathcal{L}_{\text{txt}}$	Loss Terms			UniDiffuser			BLIP-2			LLaVA		
	$\mathcal{L}_{\text{anc}}$	$\mathcal{L}_{\text{feat}}$	$\mathcal{L}_{\text{mid}}$	Ens.	$\text{ASR}_{\text{fool}}$	$\text{ASR}_{\text{target}}$	Ens.	$\text{ASR}_{\text{fool}}$	$\text{ASR}_{\text{target}}$	Ens.	$\text{ASR}_{\text{fool}}$	$\text{ASR}_{\text{target}}$
✓				0.6650	91.10%	48.20%	0.7505	93.50%	70.60%	0.5132	67.70%	27.60%
✓	✓			0.7545	99.40%	83.20%	0.7844	95.70%	83.30%	0.6107	87.70%	66.10%
✓		✓		0.7393	99.30%	84.90%	0.8049	<b>99.30%</b>	92.30%	0.6825	<b>99.90%</b>	92.90%
✓			✓	0.7375	98.20%	78.20%	0.7770	96.30%	83.30%	0.6076	86.80%	62.60%
✓	✓	✓		0.7675	99.60%	88.80%	0.8244	<b>99.30%</b>	<b>95.70%</b>	0.7025	99.80%	96.20%
✓	✓		✓	0.7551	99.50%	83.70%	0.8049	97.10%	85.10%	0.6149	88.10%	65.30%
✓	✓	✓	✓	<b>0.7705</b>	<b>99.80%</b>	<b>89.40%</b>	<b>0.8282</b>	<b>99.40%</b>	<b>94.70%</b>	<b>0.7042</b>	99.60%	<b>96.40%</b>

confirming that SGAI, HVSA, and CLSS are complementary for crafting transferable targeted adversarial examples.

#### F. Hyperparameter Selection

**Anchor Settings ( $K$  and  $\tau$ ).** We investigate the influence of the anchor count  $K$  and temperature  $\tau$  on the UniDiffuser. As shown in Fig. 6, introducing even a single anchor ( $K = 1$ ) boosts the Ensemble CLIP Score from the baseline 0.6970 to 0.7418. The performance peaks at  $K = 5$  but degrades slightly with larger  $K$ , as excessive anchors introduce less relevant anchors. Regarding  $\tau$ , extreme values lead to suboptimal weighting: small  $\tau$  yields an overly sharp distribution that underutilizes the semantic diversity of the anchor set, while large  $\tau$  produces an overly uniform distribution, failing to emphasize the most semantically relevant anchors. The results find  $\tau = 5$  as the optimal balance. Thus, we adopt  $K = 5$  and  $\tau = 5$  as the default settings.

**Hierarchical Structure (Layers).** We evaluate layer selection on UniDiffuser (ViT-B) in Fig. 7. Multi-layer alignment consistently outperforms single-layer baselines, among the tested combinations, using 3-layers achieves the best performance.

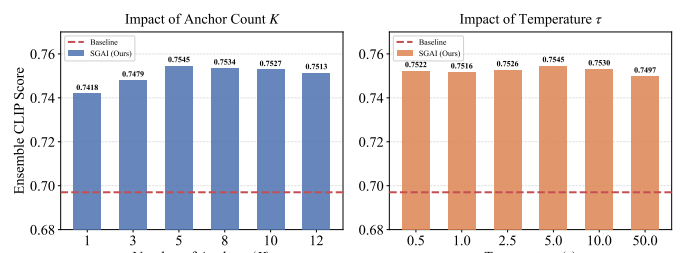


Fig. 6: Impact of hyperparameter  $K$  and  $\tau$  settings on attack performance evaluated on UniDiffuser.

Aligning only the deepest consecutive layers is suboptimal, whereas selecting layers from the latter half of the network yields the best transferability, in particular,  $\{7, 9, 11\}$  achieves the highest score. Motivated by this, we adopt a deep-layer uniform sampling strategy that selects uniformly spaced layers in the upper blocks (e.g.,  $\{7, 9, 11\}$  for ViT-B,  $\{14, 18, 22\}$  for ViT-L, and  $\{23, 30, 37\}$  for ViT-G). Additional experiments on BLIP-2 and LLaVA (Fig. 8) show that these selections

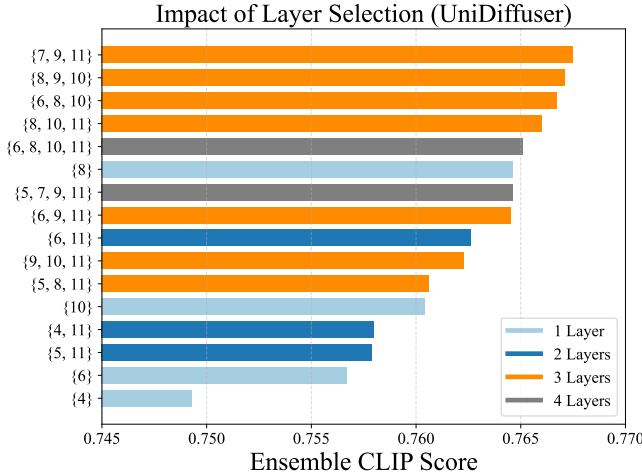


Fig. 7: Ablation study on layer selection.

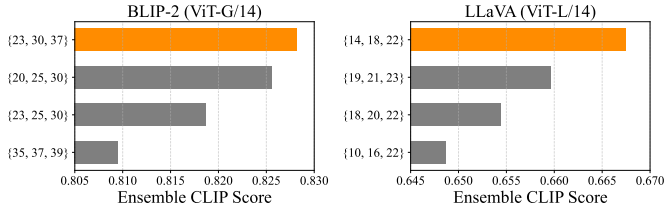


Fig. 8: Validation of the strategy on different architectures.

consistently outperform other heuristic choices, validating the generality of our strategy across architectures.

#### G. Efficiency Analysis

We conduct a runtime efficiency comparison to evaluate the computational cost of our method against state-of-the-art baselines using a single NVIDIA A100 GPU. As shown in Table VII, our method achieves a favorable trade-off between attack performance and efficiency during the optimization phase. Specifically, generating an adversarial image requires only 6.58 seconds. While slightly slower than the more efficient baselines MF-it and MF-ii due to the additional computations from hierarchical alignment, our method is significantly faster than other strong baselines, being approximately 2.8 $\times$  faster than COA (18.36s) and nearly 10 $\times$  faster than OPS (65.33s). This indicates that our method delivers state-of-the-art transferability with a modest computational overhead.

## V. CONCLUSION

This work demonstrates that targeted, surrogate-driven perturbations can reliably steer the outputs of diverse VLMs, and that improving cross-modal control requires going beyond final-layer embedding matching. Existing targeted transfer attacks commonly narrow guidance to a single target reference and focus optimization on the final layer, which makes the optimization sensitive to the surrogate-specific embedding space and leaves intermediate semantics underutilized when transferring across heterogeneous VLMs.

TABLE VII: Average attack runtime (seconds) per optimization step and per adversarial image.

Category	Method	Time/step (s)	Time/image (s)
Unrestricted	AdvDiffVLM [16]	–	60.0219
Perturbation Constrained	BSR [49]	0.1249	12.5132
	OPS [32]	0.6527	65.3270
	M-Attack [15]	0.0729	7.3433
	MF-it [13]	<b>0.0249</b>	<b>2.5007</b>
	MF-ii [13]	<b>0.0287</b>	<b>2.8812</b>
	COA [14]	0.1829	18.3643
	<b>Ours</b>	0.0656	6.5801

To overcome these issues, we develop SGHA-Attack by combining anchor-based guidance with multi-granularity alignment. Rather than optimizing toward a single reference, the attack constructs a visually grounded reference pool and uses a weighted mixture to provide stable target guidance. To enforce hierarchical consistency, the attack aligns intermediate visual features at both global and spatial granularities across multiple depths, and further synchronizes visual and textual features within a shared latent subspace. This ensures that cross-modal supervision is injected early in the pipeline rather than being restricted to the final projection.

Evaluations on both open-source and commercial black-box VLMs confirm that this design yields stronger targeted transferability and maintains robustness under common pre-processing and purification defenses. While highly effective, the improvements can be less pronounced on advanced commercial systems that incorporate proprietary defense policies and complex transformations, motivating future work on more adaptive transfer strategies for such policy-rich black-box settings. Ultimately, these results highlight the need for defenses that explicitly safeguard internal feature hierarchies against semantic-level hijacking.

## REFERENCES

- [1] J. Zhang, J. Huang, S. Jin *et al.*, “Vision-language models for vision tasks: A survey,” *IEEE Transactions on Pattern Analysis and Machine Intelligence*, vol. 46, no. 8, pp. 5625–5644, 2024.
- [2] J. Li, D. Li, C. Xiong *et al.*, “BLIP: bootstrapping language-image pre-training for unified vision-language understanding and generation,” in *International Conference on Machine Learning*, 2022, pp. 12 888–12 900.
- [3] H. Liu, C. Li, Q. Wu *et al.*, “Visual instruction tuning,” in *Advances in Neural Information Processing Systems*, 2023.
- [4] J. Zhou, T. Lu, S. Mishra *et al.*, “Instruction-following evaluation for large language models,” *arXiv preprint arXiv:2311.07911*, 2023.
- [5] Z. Xu, Y. Zhang, E. Xie *et al.*, “Drivegpt4: Interpretable end-to-end autonomous driving via large language model,” *IEEE Robotics and Automation Letters*, vol. 9, no. 10, pp. 8186–8193, 2024.
- [6] M. Moor, O. Banerjee, Z. S. H. Abad *et al.*, “Foundation models for generalist medical artificial intelligence,” *Nature*, vol. 616, no. 7956, pp. 259–265, 2023.
- [7] D. Liu, M. Yang, X. Qu *et al.*, “A survey of attacks on large vision-language models: Resources, advances, and future trends,” *IEEE Transactions on Neural Networks and Learning Systems*, vol. 36, no. 11, pp. 19 525–19 545, 2025.
- [8] Y. Dong, H. Chen, J. Chen *et al.*, “How robust is google’s bard to adversarial image attacks?” *arXiv preprint arXiv:2309.11751*, 2023.
- [9] X. Qi, K. Huang, A. Panda *et al.*, “Visual adversarial examples jailbreak aligned large language models,” in *AAAI Conference on Artificial Intelligence*, 2024, pp. 21 527–21 536.

[10] J. Gu, X. Jia, P. de Jorge *et al.*, “A survey on transferability of adversarial examples across deep neural networks,” *Transactions on Machine Learning Research*, vol. 2024, 2024.

[11] K. Greshake, S. Abdelnabi, S. Mishra, *et al.*, “Not what you’ve signed up for: Compromising real-world llm-integrated applications with indirect prompt injection,” in *ACM Workshop on Artificial Intelligence and Security*, 2023, pp. 79–90.

[12] C. H. Wu, J. Y. Koh, R. Salakhutdinov *et al.*, “Adversarial attacks on multimodal agents,” *arXiv preprint arXiv:2406.12814*, 2024.

[13] Y. Zhao, T. Pang, C. Du *et al.*, “On evaluating adversarial robustness of large vision-language models,” in *Advances in Neural Information Processing Systems*, vol. 36, 2023, pp. 54 111–54 138.

[14] P. Xie, Y. Bie, J. Mao *et al.*, “Chain of attack: On the robustness of vision-language models against transfer-based adversarial attacks,” in *IEEE/CVF Conference on Computer Vision and Pattern Recognition*, 2025, pp. 14 679–14 689.

[15] Z. Li, X. Zhao, D.-D. Wu *et al.*, “A frustratingly simple yet highly effective attack baseline: Over 90% success rate against the strong black-box models of gpt-4.5/4o/01,” *arXiv preprint arXiv:2503.10635*, 2025.

[16] Q. Guo, S. Pang, X. Jia *et al.*, “Efficient generation of targeted and transferable adversarial examples for vision-language models via diffusion models,” *IEEE Transactions on Information Forensics and Security*, vol. 20, pp. 1333–1348, 2025.

[17] J. Achiam, S. Adler, S. Agarwal *et al.*, “GPT-4 technical report,” *arXiv preprint arXiv:2303.08774*, 2023.

[18] G. Team, R. Anil, S. Borgeaud *et al.*, “Gemini: A family of highly capable multimodal models,” *arXiv preprint arXiv:2312.11805*, 2023.

[19] K.-H. Lee, X. Chen, G. Hua *et al.*, “Stacked cross attention for image-text matching,” in *European Conference on Computer Vision*, 2018, pp. 212–228.

[20] Y.-C. Chen, L. Li, L. Yu *et al.*, “UNITER: universal image-text representation learning,” in *European Conference on Computer Vision*, 2020, pp. 104–120.

[21] P. Anderson, X. He, C. Buehler *et al.*, “Bottom-up and top-down attention for image captioning and visual question answering,” in *IEEE/CVF Conference on Computer Vision and Pattern Recognition*, 2018, pp. 6077–6086.

[22] Y. Goyal, T. Khot, D. Summers-Stay *et al.*, “Making the V in VQA matter: Elevating the role of image understanding in visual question answering,” in *IEEE/CVF Conference on Computer Vision and Pattern Recognition*, 2017, pp. 6325–6334.

[23] W. X. Zhao, K. Zhou, J. Li *et al.*, “A survey of large language models,” *arXiv preprint arXiv:2303.18223*, 2023.

[24] C. Zhou, Q. Li, C. Li *et al.*, “A comprehensive survey on pretrained foundation models: A history from BERT to chatgpt,” *International Journal of Machine Learning and Cybernetics*, vol. 16, no. 12, pp. 9851–9915, 2025.

[25] H. Touvron, T. Lavig, G. Izacard *et al.*, “Llama: Open and efficient foundation language models,” *arXiv preprint arXiv:2302.13971*, 2023.

[26] W.-L. Chiang, Z. Li, Z. Lin *et al.*, “Vicuna: An open-source chatbot impressing gpt-4 with 90%\* chatgpt quality,” See <https://vicuna.lmsys.org>, 2023.

[27] D. Zhu, J. Chen, X. Shen *et al.*, “Minigpt-4: Enhancing vision-language understanding with advanced large language models,” in *International Conference on Learning Representations*, 2024.

[28] J. Li, D. Li, S. Savarese *et al.*, “BLIP-2: bootstrapping language-image pre-training with frozen image encoders and large language models,” in *International Conference on Machine Learning*, 2023, pp. 19 730–19 742.

[29] W. Dai, J. Li, D. Li *et al.*, “Instructblip: Towards general-purpose vision-language models with instruction tuning,” in *Advances in Neural Information Processing Systems*, 2023.

[30] I. J. Goodfellow, J. Shlens, and C. Szegedy, “Explaining and harnessing adversarial examples,” in *International Conference on Learning Representations*, 2015.

[31] N. Carlini and D. A. Wagner, “Towards evaluating the robustness of neural networks,” in *IEEE Symposium on Security and Privacy*, 2017, pp. 39–57.

[32] Y. Guo, W. Liu, Q. Xu *et al.*, “Boosting adversarial transferability through augmentation in hypothesis space,” in *IEEE/CVF Conference on Computer Vision and Pattern Recognition*, 2025, pp. 19 175–19 185.

[33] X. Wang, X. He, J. Wang *et al.*, “Admix: Enhancing the transferability of adversarial attacks,” in *IEEE/CVF International Conference on Computer Vision*, 2021, pp. 16 138–16 147.

[34] C. Xie, Z. Zhang, Y. Zhou *et al.*, “Improving transferability of adversarial examples with input diversity,” in *IEEE/CVF Conference on Computer Vision and Pattern Recognition*, 2019, pp. 2730–2739.

[35] H. Wang, W. Luo, X. Xie *et al.*, “Adv-inversion: Stealthy adversarial attacks via gan-inversion for facial privacy protection,” *IEEE Transactions on Information Forensics and Security*, vol. 20, pp. 11 892–11 906, 2025.

[36] X. Jia, S. Gao, S. Qin *et al.*, “Adversarial attacks against closed-source mllms via feature optimal alignment,” *arXiv preprint arXiv:2505.21494*, 2025.

[37] Z. Chen, B. Li, S. Wu *et al.*, “Query-efficient decision-based black-box patch attack,” *IEEE Transactions on Information Forensics and Security*, vol. 18, pp. 5522–5536, 2023.

[38] H. Wang, K. Dong, Z. Zhu *et al.*, “Transferable multimodal attack on vision-language pre-training models,” in *IEEE Symposium on Security and Privacy*, 2024, pp. 1722–1740.

[39] X. Cui, A. Aparcero, Y. K. Jang *et al.*, “On the robustness of large multimodal models against image adversarial attacks,” in *IEEE/CVF Conference on Computer Vision and Pattern Recognition*, 2024, pp. 24 625–24 634.

[40] J. Zhang, Q. Yi, and J. Sang, “Towards adversarial attack on vision-language pre-training models,” in *ACM International Conference on Multimedia*, 2022, pp. 5005–5013.

[41] D. Lu, Z. Wang, T. Wang *et al.*, “Set-level guidance attack: Boosting adversarial transferability of vision-language pre-training models,” in *IEEE/CVF International Conference on Computer Vision*, 2023, pp. 102–111.

[42] Y. Wang, C. Liu, Y. Qu *et al.*, “Break the visual perception: Adversarial attacks targeting encoded visual tokens of large vision-language models,” in *ACM International Conference on Multimedia*, 2024, pp. 1072–1081.

[43] Y. Cao, Y. Li, K. Liang *et al.*, “Enhancing targeted adversarial attacks on large vision-language models via intermediate projector,” *arXiv preprint arXiv:2508.13739*, 2025.

[44] J. Deng, W. Dong, R. Socher *et al.*, “Imagenet: A large-scale hierarchical image database,” in *IEEE Conference on Computer Vision and Pattern Recognition*, 2009, pp. 248–255.

[45] T.-Y. Lin, M. Maire, S. J. Belongie *et al.*, “Microsoft COCO: common objects in context,” in *European Conference on Computer Vision*, 2014, pp. 740–755.

[46] R. Rombach, A. Blattmann, D. Lorenz *et al.*, “High-resolution image synthesis with latent diffusion models,” in *IEEE/CVF Conference on Computer Vision and Pattern Recognition*, 2022, pp. 10 674–10 685.

[47] F. Bao, S. Nie, K. Xue *et al.*, “One transformer fits all distributions in multi-modal diffusion at scale,” in *International Conference on Machine Learning*, 2023, pp. 1692–1717.

[48] H. Liu, C. Li, Y. Li *et al.*, “Llava-next: Improved reasoning, ocr, and world knowledge,” 2024. [Online]. Available: <https://llava-vl.github.io/blog/2024-01-30-llava-next/>

[49] K. Wang, X. He, W. Wang *et al.*, “Boosting adversarial transferability by block shuffle and rotation,” in *IEEE/CVF Conference on Computer Vision and Pattern Recognition*, 2024, pp. 24 336–24 346.

[50] Z. Wang, A. C. Bovik, H. R. Sheikh *et al.*, “Image quality assessment: from error visibility to structural similarity,” *IEEE Transactions on Image Processing*, vol. 13, no. 4, pp. 600–612, 2004.

[51] A. Madry, A. Makelov, L. Schmidt *et al.*, “Towards deep learning models resistant to adversarial attacks,” in *International Conference on Learning Representations*, 2018.

[52] W. Xu, D. Evans, and Y. Qi, “Feature squeezing: Detecting adversarial examples in deep neural networks,” in *Annual Network and Distributed System Security Symposium*, 2018.

[53] G. K. Dziugaite, Z. Ghahramani, and D. M. Roy, “A study of the effect of JPG compression on adversarial images,” *arXiv preprint arXiv:1608.00853*, 2016.

[54] X. Jia, X. Wei, X. Cao *et al.*, “Comdefend: An efficient image compression model to defend adversarial examples,” in *IEEE/CVF Conference on Computer Vision and Pattern Recognition*, 2019, pp. 6084–6092.

[55] W. Nie, B. Guo, Y. Huang *et al.*, “Diffusion models for adversarial purification,” in *International Conference on Machine Learning*, 2022, pp. 16 805–16 827.